

Degradation mechanism of high-voltage single-crystal $LiNi_{0.5}Co_{0.2}Mn_{0.3}O_2$ cathode material

Na Liu(柳娜)
Citation: Chin. Phys. B, 2023, 32 (**12**): 128202. DOI: 10.1088/1674-1056/ad01a3
Journal homepage: http://cpb.iphy.ac.cn; http://iopscience.iop.org/cpb

What follows is a list of articles you may be interested in

Synthesis and electrochemical performance of La_2CuO_4 as a promising coating material for high voltage Li-rich layered oxide cathodes

Fuliang Guo(郭福亮), Jiaze Lu(卢嘉泽), Meihua Su(苏美华), Yue Chen(陈约), Jieyun Zheng(郑杰允), Liang Yin(尹良), and Hong Li(李泓)
Chin. Phys. B, 2023, 32 (**8**): 088201. DOI: 10.1088/1674-1056/acd2bc

Electron density distribution of $LiMn_2O_4$ cathode investigated by synchrotron powder x-ray diffraction

Tongtong Shang(尚彤彤), Dongdong Xiao(肖东东), Qinghua Zhang(张庆华), Xuefeng Wang(王雪锋), Dong Su(苏东), and Lin Gu(谷林)
Chin. Phys. B, 2021, 30 (**7**): 078202. DOI: 10.1088/1674-1056/abf347

Neutron-based characterization techniques for lithium-ion battery research

Enyue Zhao(赵恩岳), Zhi-Gang Zhang(张志刚), Xiyang Li(李西阳), Lunhua He(何伦华), Xiqian Yu(禹习谦), Hong Li(李泓), Fangwei Wang(王芳卫)
Chin. Phys. B, 2020, 29 (**1**): 018201. DOI: 10.1088/1674-1056/ab5d07

Improved electrochemical performances of high voltage $LiCoO_2$ with tungsten doping

Jie-Nan Zhang(张杰男), Qing-Hao Li(李庆浩), Quan Li(李泉), Xi-Qian Yu(禹习谦), Hong Li(李泓)
Chin. Phys. B, 2018, 27 (**8**): 088202. DOI: 10.1088/1674-1056/27/8/088202

Instability of lithium bis(fluorosulfonyl)imide (LiFSI)–potassium bis(fluorosulfonyl)imide (KFSI) system with $LiCoO_2$ at high voltage

Zhang Shu (张舒), Li Wen-Jun (李文俊), Ling Shi-Gang (凌仕刚), Li Hong (李泓), Zhou Zhi-Bin (周志彬), Chen Li-Quan (陈立泉)
Chin. Phys. B, 2015, 24 (**7**): 078201. DOI: 10.1088/1674-1056/24/7/078201

Degradation mechanism of high-voltage single-crystal $LiNi_{0.5}Co_{0.2}Mn_{0.3}O_2$ cathode material

Na Liu(柳娜)†

Contemporary Amperex Technology Co., Limited, Ningde 352000, *China*

(Received 24 July 2023; revised manuscript received 22 September 2023; accepted manuscript online 10 October 2023)

Layered cathode materials have been successfully commercialized and applied to electric vehicles. To further improve improve the energy density of these marterials is still the main efforts in the market. Therefore, developing high-voltage $LiNi_xCo_yMn_zO_2$ ($x+y+z=1$, NCM) to achieve high energy density is particularly important. However, under high voltage cycling, NCM often exhibits rapid capacity degradation, which can be attributed to oxygen release, structural phase transition and particle cracking. In this work, the representative single-crystal $LiNi_{0.5}Co_{0.2}Mn_{0.3}O_2$ (NCM523) was studied under various high charge cut-off voltages. Analysis by x-ray diffraction (XRD), transmission electron microscope (TEM) and electron back scatter diffraction (EBSD) measurements indicated that the rock-salt phase is formed on the surface of the particles after high voltage cycling, which is responsible for the increase of impedance and the rapid decay of capacity. Therefore, inhibiting the formation of rock-salt phase is believed an effective strategy to address the failure of NCM under high voltages. These findings provide effective guidance for the development of high-voltage NCM.

Keywords: high voltage, Li-ion battery, phase transition, $LiNi_xCo_yMn_zO_2$

PACS: 82.45.–h, 82.45.Yz **DOI:** 10.1088/1674-1056/ad01a3

1. Introduction

Since the development of $LiCoO_2$ for commercial applications, high energy density, high safety, long life and low cost are the demands for a new generation of lithium-ion batteries. The $LiNi_xCo_yMn_zO_2$ ($x+y+z=1$; NCM; 280 mAh/g) has a higher theoretical specific capacity than $LiFePO_4$ (170 mAh/g) and $LiMn_2O_4$ (150 mAh/g), which may become the most powerful competitor in the new generation of battery materials.[1–4] The safety and stability of NCM can be improved by adjusting the atomic ratio of transition metals (TMs), which has been successfully applied in mobile electronic devices and power vehicles. In order to improve the energy density, Ni-rich and Co-poor NCMs have been widely developed and applied, but the cycle performance is seriously affected due to a series of side reactions and irreversible phase transitions. Therefore, recent attention is focused on adjusting the charge cut-off voltage of NCM and optimizing the electrolyte composition to obtain higher energy density. However, at high operating voltage (>4.4 V), the charge compensation process of NCM could be changed due to the deep lithium removal. At lower voltages (<4.4 V), TM participates in the charge compensation by valence change, while at higher voltages (>4.4 V), the anions participate in charge compensation to form peroxide ($O_2^{\sigma-}$) or oxygen.[5] In addition, Li^+ extraction will aggravate Li/Ni mixing and result in irreversible phase transition generating spinel phase and rock-salt phase.[6,7] The dissolution of transition metal[8] and particle cracking due to inhomogeneous stress distribution[9–13] also restrict the applications of high voltage NCM.

In this paper, the commercial single-crystal $LiNi_{0.5}Co_{0.2}Mn_{0.3}O_2$ (NCM523) was used to investigate the cycle performance under different charging cut-off voltages. The crystal structure and surface phase transition process of NCM523 after high voltage cycling were investigated by means of x-ray diffraction (XRD), transmission electron microscope (TEM) and electron back scatter diffraction (EBSD), and the surface structure degradation under different cut-off voltages was understood for improving the performance of NCM materials under high voltages.

2. Experimental materials and equipment

The tested electrode was made of commercial single crystal NCM523 material, mixed with an appropriate amount of conductive carbon and binder (PVDF) dissolved in NMP, and coated on the surface of Al foil. The full battery used graphite as anode, NCM523 as cathode, 1 M $LiPF_6$ in EC/DMC (1:1 vol/vol) as electrolyte. The charging and discharging process was carried out at 0.33 C between 2.8–4.4 V, 2.8–4.5 V and 2.8–4.6 V. All cycling tests were performed on a NEWARE battery tester, and the EIS test was performed on an AutoLab electrochemical workstation (frequency range of 1 MHz to 1 mHz). The XRD test was conducted on Bruker D8, with Cu $K\alpha$ as the radiation source, the scanning range was 15°–85°, and the scanning speed was 5 °/min. the cross-sections of the particles were polished using a cooling cross-section polisher (IB-19520CCP, JEOL). The TEM sample was fabricated by the focused ion beam (FIB) on Scios DualBeam double-beam electron microscope. All TEM tests were per-

†Corresponding author. E-mail: LiuN@CATL.com

© 2023 Chinese Physical Society and IOP Publishing Ltd

formed on the JEM2100 equipment produced by Nippon Electronics. Scanning electron microscope (SEM) test was performed on the field emission scanning electron microscope Zeiss Gemini360. EBSD was performed using the Oxford Nordly max3.

3. Results

3.1. Electrochemical performance

Figure 1(a) shows the charge–discharge cycle curve of NCM523 half-cell at 0.05 C (1 C = 6.6 mA), the specific capacity of NCM523 at 4.55 V is 170 mAh/g for the initial cycle. The capaciy decays faster in the accelerated decaying test (45 °C) as the charge cut-off voltage increases from 4.4 V to 4.6 V. Especially at 4.6 V, capacity fade to less than 80% around 150 cycles, as shown in Fig. 1(b). To eliminate the influence of the dynamics factors, the half cell was further discharged to 2.85 V at very low rate of 0.04 C after discharging from 0.33 C to 2.85 V. After 150 cycles at the cut off voltages of 4.4/4.5/4.6 V, the half-cell was cycled at 0.33 + 0.04 C, and the power capacity loss was obtained (0.33 C), as shown in Fig. 2(a). There is basically no irreversible capacity loss after 150 cycles at 2.8–4.4 V. For the 2.8–4.5 V cycle, the capacity loss is 12.9% at 150 cycles, most of which is caused by the reversible capacity loss (10.05%). The capacity loss is the largest after 150 cycles of 2.8–4.6 V cycle, reaching 29.2% (0.33 C+0.04 C), of which irreversible loss accounts for 14.24% and power loss accounts for 14.95%. It can be seen that the higher the cycle voltage results in the larger the capacity loss, and it mainly comes from the power loss. The reversible loss is mainly considered to be the slowing down of the kinetic process. The power loss is often considered to be the capacity attenuation caused by the loss of active materials. Figure 2(b) show the dissolved TMs ions on the negative electrode of samples after 150 cycles at different cut-off voltages detected by inductively coupled plasma-optical emission spectrometer (ICP-OES). The results show the sample at low cut-off voltage has much less TMs ions dissolution. Although the amount of Mn dissolved is the largest, the overall amount of TMs dissolved are relatively small. Therefore, the dissolution of TMs is not the main reason for capacity decay.

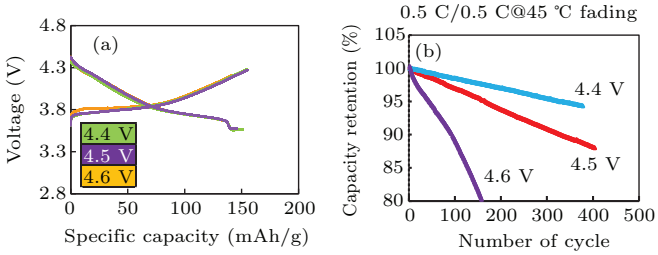


Fig. 1. NCM523 cycle performance. (a) 0.05 C charge–discharge curve of NCM523 half-cells at different cut-off voltages. (b) The capacity retention curves with different cut-off voltages at 45 °C (4.4 V, 4.5 V, 4.6 V).

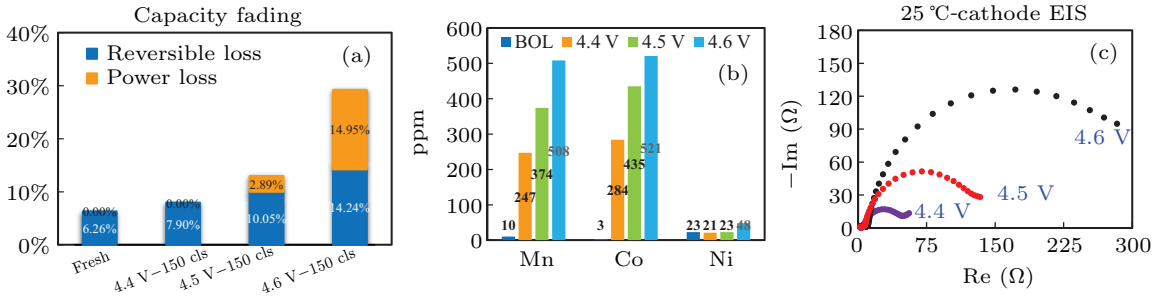


Fig. 2. (a) Capacity loss of half-cells (Li||NCM) under different cut-voltages. (b) The dissolved TMs ions on the negative electrode after 150 cycles. (c) After the pole piece is disassembled, the positive pole piece is made into a symmetrical battery EIS curve.

Electrochemical impedance spectroscopy (EIS) analysis was performed on the symmetrical battery made of the disassembled NCM523 electrode to study the interfacial impedance change. Figure 2(c) shows the relationship between the impedance change and the cut-off voltage. An obvious semicircle can be observed, corresponding to the electron transfer process (R_{ct}). According to the results, R_{ct} at 4.6 V is much larger than that at the lower charge cut-off voltages (4.4 V and 4.5 V) during cycling. The surface film impedance R_f varies less with the cut-off voltages relative to R_{ct}, which can be ignored here. It can be seen that the capacity attenuation during cycling at high voltages may be related to the increase in the charge transfer impedance (R_{ct}) of the electrodes. In the following discussion, we will focus on the origin of the increased charge transfer resistance of the samples cycled at high charge cut-off voltages by analyses that consider both the bulk and surface structure.

3.2. Phase transition behavior

In order to study the reason of capacity decay during high voltage cycling, the bulk structure of NCM523 after cycling was first examined using XRD. Each sample at the discharged state (2.8 V) after 150 cycles was collected and analyzed. By comparison, it is found that all the samples show the hexagonal α-$NaFeO_2$ structure of the R-3m space group, and no significant structural degradation and new phase formation was observed (Fig. 3). It is known that Ni^{2+} (0.69 Å) and Li^{+}(0.76 Å) are similar in the atomic radius. In the NCM, the Li vacancy (3b site) left in the Li slab after Li^{+} extraction is

easily occupied by Ni^{2+}, forming the "cationic mixed phase" or "cation disorder".[14] The ratio of (003) diffraction peak intensity to (104) diffraction peak intensity $I_{(003)/(104)}$ is often used to analyze the degree of cation mixing in the XRD spectrum. The smaller is the value of $I_{(003)/(104)}$, the more severe is the cation mixing.[15] A large number of studies have shown that the cation mixing facilitates the blocking of the Li^+ channel due to the larger diffusion barriers in the Li layers. It can be seen that a higher degree of cation mixing was observed for samples that were operated at higher voltages. This indicates that the electrode polarization becomes more severe when cycled at high voltages consistent with the larger resistance value (Fig. 2(c)).[16,17]

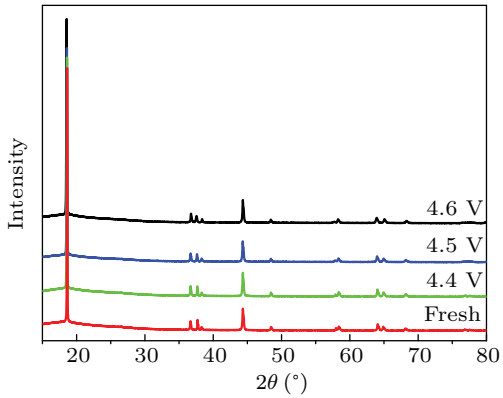


Fig. 3. Comparison of XRD patterns before and after 150 cycles of high voltage cycling.

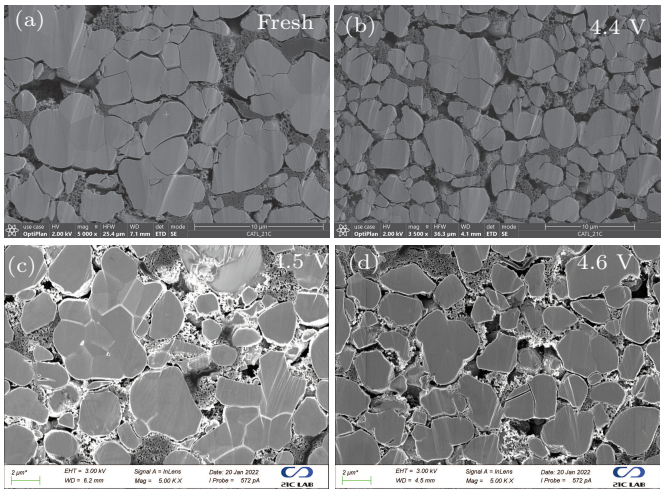


Fig. 4. SEM images before and after high voltage cycle. (a) The cross-sectional SEM image of fresh electrode. (b)–(d) The cross-sectional SEM images after 150 cycles at different cut-off voltages.

During the charging process, the NCM usually undergoes a series of phase change. For example, in the single-crystal NCM811 system, the phase transition sequence between 2.8 V and 4.6 V is H1→M→H2→H3.[15] In addition, in the process of charging and discharging, the lattice expansion and contraction generate increased micro-stress, resulting in micro-cracks in the particle, and deteriorating the electronic conductivity.[11] The electrolyte enters the interior of the particle via these crack networks and decomposes to form CEI, which affects the transport of electrons and ions at the interface. The SEM was carried out to observe the cross-sections of the electrode at different cut-off voltages. Figure 4 shows the SEM images of the full-discharged NCM523 (particle size is about 2–5 μm) before and after the cycle. It can be observed that the particles remain intact even in the 2.8–4.6 V cycle, and there is no particle cracking, suggesting that the reason for the rapid attenuation of capacity at high voltage is not related to the micro-cracks of particles.

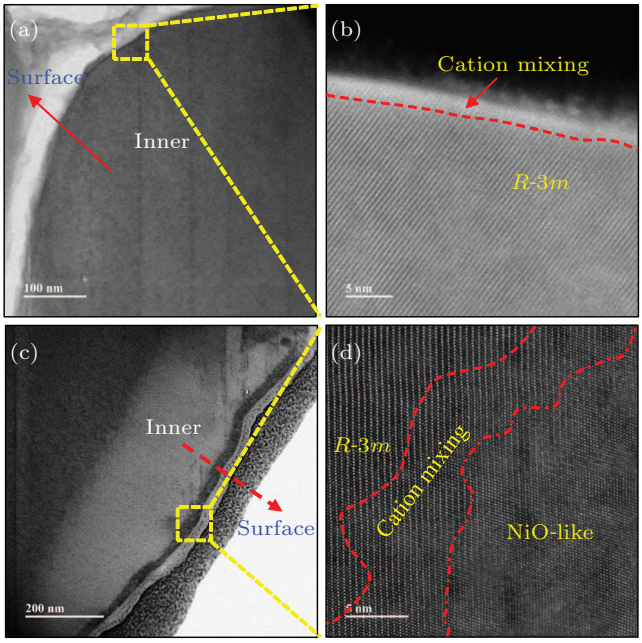


Fig. 5. Atomic resolution STEM images of NCM523 after different cut-off voltages. The HADDF-STEM images of (a), (b) 2.8–4.5 V after 150 cycles. (b) The high-resolution STEM image indicated by yellow dotted rectangle in (a). (c), (d) STEM images after 150 cycles under 2.8–4.6 V conditions 150 cycles. (d) The high-resolution STEM image indicated by yellow dotted rectangle in (c).

The above XRD data analysis indicates that the $I_{(003)/(104)}$ value decreases with the increase of the cut-off voltage, demonstrating that the cation mixing is more severe at high voltage. It was reported that the particle surface contact with the electrolyte is prone to the phase transition of the layered structure, from the layered *R*-3*m* to the rock-salt phase NiO-like (*Fm*-3*m*) or the spinel-like phase, thereby destroying the active Li site, blocking the lithium intecalation channel, and decreasing the ionic conductivity.[17,18] In order to further explore the surface structure phase transition and cation mixing phase, the HADDF-STEM analyses were performed. After 150 cycles, the cation mixed phase with a thickness of about 2 nm appeared on the surface of NCM cycled between 2.8–4.5 V (Figs. 5(a) and 5(b)). The thickness of the surface cation mixed phase is larger after 4.6 V cycling than 4.5 V cycling. Meanwhile, a reconstruction layer of 5–10 nm appears on the outermost surface and along the lithium diffusion channels. The high-resolution STEM can clearly recognize the reconstructed layer as a rock-salt phase(NiO) structure (Figs. 5(c)

and 5(d). Since the STEM imaging is located, in order to further count the distribution of salt rock phase, the argon ion beam was applied to polish the cathodes after the 2.8–4.6 V cycling, and the smooth and clean surface is obtained. EBSD test can observe a wide range of crystal structure phase transition (Fig. 6). For the as-prepared cathodes, the EBSD results showed that the crystal plane orientation was relatively random, without obvious meritocratic orientation, and the particles were of single crystal type, with well-defined grains and agglomerates inside the particles. For the samples after 2.8–4.6 V cycling, the rock-salt phase (NiO) appears and has a special orientation relationship with the layered structure, which is consistent with the above STEM results.

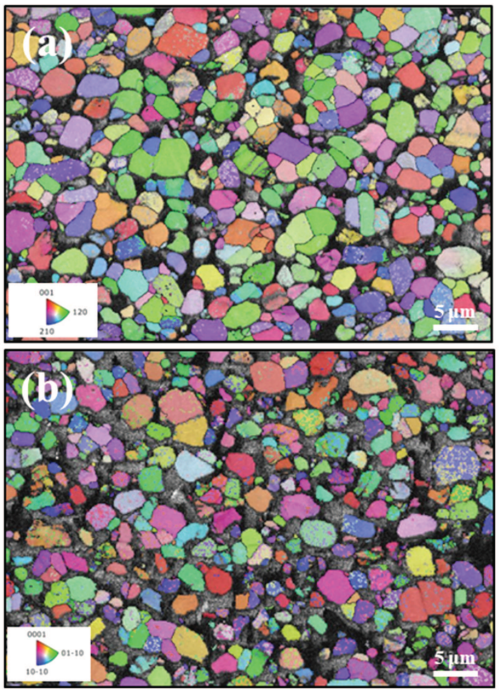


Fig. 6. EBSD images of (a) fresh NCM523 electrode and (b) after 150 cycles under 2.8–4.6 V. The color represents crystal direction. As for fresh electrode, each particle contains only one color, which represents a single crystal particle. The particles contain other crystal orientations, indicating phase transformation after cycling.

The formation of surface rock-salt phase is related to cation exchange and cation migration, which is attributed to the similar radius of Li^+ and Ni^{2+}, and the low energy barrier of Li^+/Ni^{2+} exchange, which is easy to occur in NCM. The process of Li^+/Ni^{2+} cation mixing and Ni^{2+} migration is related to the formation of Li vacancies after extracting lithium from NCM, and the above process occurs most obviously when more lithium is extracted at high voltage.[18] During the charging process, Li^+ is gradually removed from the particle surface. The Li-removed NCM is thermodynamically unstable, and the surface oxygen is active and is lost at high voltage. Since the formation energy of Li/Ni mixing in NCM is relatively lower than that of Li/Co or Li/Mn, a large amount of cation exchange between Li/Ni occurs in NCM, and then the Ni atoms that are located in Li layers, migrated to the particle surface, leading to the enrichment of Ni on the non-(001) surface and the growth of rock-salt phase in the reconstructed layer.[19–21] The formation of salt rock phase leads to the loss of active Li sites, and hinders the lithium diffusion. The variation of charge transfer resistance above 4.4 V can be attributed to the rock-salt or cation mixing phase that exist more profoundly on the surface of the 4.6 V charged samples than on the 4.4 V charged sample.[22,23]

Elemental doping is feasible for preparing layered materials with high-voltage stability. Doping elements into the material lattice can enhance the O–TM bonding, improving the structural stability and suppressing the oxygen release. As mentioned above, the electrolyte decomposition at active material surface significantly affects the performance of the cathodes at high charge voltages. Surface coating can act as a physical protection barrier to isolate the active materials from the electrolyte and inhibit the generation of CEI at high working voltage. The common coating materials mainly contain oxides,[24,25] phosphates[26] and fluorides.[27]

4. Conclusion

In this paper, NCM523 is used to explore the cycle performance under different cut-off voltages (2.8–4.4 V, 2.8–4.5 V and 2.8–4.6 V). Under the condition of 45 °C as the acceleration factor, the higher is the cut-off voltage, the faster will be the capacity decay. Among them, the capacity of the 4.6 V charged material decays by 80% after 150 cycles, which is due to power loss. Further analysis shows that the R_{ct} undergoes a substantially larger increase during cycling at high voltages. Combined with XRD and STEM, it was found that there was no obvious phase transition and cracking in the bulk of the material. High-resolution STEM and EBSD confirmed that the layered structure on the surface of the particles changed to the mixed phase or rock-salt phase after cycling at high voltages. Therefore, the phase transition near the surface at high voltages is mainly responsible for capacity degradation. Our understanding provides an important reference for further improving the high-voltage NCM523 performance.

References

[1] Shi J L, Xiao D D, Ge M Y, Yu X Q, Chu Y, Huang X J, Zhang X D, Yin Y X, Yang X Q, Guo Y G, Gu L and Wan L J 2018 *Adv. Mater.* **30** 1705575

[2] Zhang H, He X Z, Chen Z H, Yang Y, Xu H, Wang L and He X M 2022 *Adv. Energy Mater.* **12** 2202022

[3] Ni L S, Zhang S, Di A D, Deng W T, Zou G Q, Hou H S and Ji X B 2022 *Adv. Energy Mater.* **12** 2201510

[4] Kim J, Lee H, Cha H, Yoon M, Park M and Cho J 2018 *Adv. Energy Mater.* **8** 1702028

[5] Shi C G, Peng X X, Dai P, Xiao P H, Zheng W C, Li H Y, Li H, Indris S, Mangold S, Hong Y H, Luo C X, Shen C H, Wei Y M, Huang L and Sun S G 2022 *Adv. Energy Mater.* **12** 2200569

[6] Xu C, Reeves P J, Jacquet Q and Grey C P 2020 *Adv. Energy Mater.* **11** 2003404

[7] Zhang F, Lou S F, Li S, Yu Z J, Liu Q S, Dai A, Cao C T, Toney M F, Ge M Y, Xiao X S, Lee W K, YaoY D, Deng J J, Liu T C, Tang Y P, Yin G P, Lu J, Su D and Wang J J 2020 *Nat. Commun.* **11** 3050

[8] Wandt J, Freiberg A, Thomas R, Gorlin Y, Siebel A, Jung R, Gasteigera H A and Tromp M 2016 *J. Mater. Chem. A* **4** 18300

[9] Han G M, Kim Y S, Ryu H H, Sun Y K and Yoon C S 2022 *ACS Energy Lett.* **7** 2919

[10] Ren Z M, Zhang X H, Liu M, Zhou J J, Sun S, He H Y and Wang D Y 2019 *J. Power Sources* **416** 104

[11] Yan P F, Zheng J M, Gu M, Xiao J, Zhang J G and Wang C M 2017 *Nat. Commun.* **8** 14101

[12] Bi Y J, Tao J H, Wu Y Q, Li L Z, Xu Y B, Hu E Y, Wu B B, Hu J T, Wang C M, Zhang J G, Yue Qi and Jie Xiao 2020 *Science* **370** 1313

[13] Park N Y, Park G T, Kim S B, Jung W M, Park B C and Sun Y K 2022 *ACS Energy Lett.* **7** 2362

[14] Liu W, Oh P, Liu X, Lee M J, W, Chae S, Kim Y and Cho J 2015 *Angew. Chem. Int. Ed.* **54** 4440

[15] Sun J M, Cao X,Yang H J, He P, Dato M A, Cabana J and Zhou H S 2022 *Angew. Chem. Int. Ed.* **134** 202207225

[16] Jung S K, Gwon H, Hong J, Park K Y, Seo D H, Kim H, Jangsuk Hyun, Yang W and Kang K 2014 *Adv. Energy Mater.* **4** 1300787

[17] Lin F, Markus I M, Nordlund D, Weng T C, Asta M D, Xin H L and Doeff M M 2014 *Nat. Commun.* **5** 3529

[18] Zhu J, Sharifi-Asl S, Garcia J C, Iddir H H, Croy J R, Shahbazian-Yassar R and Chen G Y 2020 *ACS Appl. Energy Mater.* **3** 4799

[19] Huang W Y, Lin C, Zhang M J, Li S N, Chen Z F, Zhao W G, Zhu C, Zhao Q, Chen H B and Pan F 2021 *Adv. Energy Mater.* **11** 2102646

[20] Tanim T R, Yang Z Z, Finegan D P, Chinnam P R, Lin Y L, Weddle P J, Bloom I, Colclasure A M, Dufek E J, Wen J G, Tsai Y F, Evans M C, Smith K, Allen J M, Dickerson C C, H. Quinn A H, Dunlop A R, Trask S E and Jansen A N 2022 *Adv. Energy Mater.* **12** 2103712

[21] Dixit H, Zhou W, Idrobo J C, Nanda J and Cooper V R 2014 *ACS Nano* **8** 2103712

[22] Zhang M J, Teng G F, Karen Y C, Chen-Wiegart, Duan Y D, Peter Ko J Y, Zheng J X, Thieme J, Dooryhee E, Chen Z H, Bai J M, Amine K, Pan F and Wang F 2018 *J. Am. Chem. Soc.* **140** 12484

[23] Zhang J C,Zhou D, Yang W Y, Yang J B, Sun L M, Schumacher G and Liu X F 2019 *J. Electrochem. Soc.* **166** A4097

[24] Uchida S, Zettsu N, Hirata K, Kamic K and Teshima K 2016 *RSC Adv.* **6** 67514

[25] Huang Y Y, Chen J T, Ni J F, Zhou H H and Zhang X X 2009 *J. Power Sources* **188** 538

[26] Song H G, Kim J Y, Kim K T and Park Y J 2011 *J. Power Sources* **196** 6847

[27] Song H G, Kim S B and Par Y J 2012 *J. Electroceram.* **29** 163